Journal of The Electrochemical Society

All Solid-State Lithium–Sulfur Battery Using a Glass-Type P_2S_5–Li_2S Electrolyte: Benefits on Anode Kinetics

All Solid-State Lithium–Sulfur Battery Using a Glass-Type P_2S_5–Li_2S Electrolyte: Benefits on Anode Kinetics

Takanobu Yamada,[a] Seitaro Ito,[a] Ryo Omoda,[a] Taku Watanabe,[a,*] Yuichi Aihara,[a,*,z] Marco Agostini,[b] Ulderico Ulissi,[b,*] Jusef Hassoun,[b] and Bruno Scrosati[c,,d]**

[a]*Samsung R&D Institute Japan, Minoh-shi, Osaka 562-0036, Japan*
[b]*Department of Chemistry, University of Rome "La Sapienza," Rome 00185, Italy*
[c]*Electrochimica ed Energia, Rome 00199, Italy*

Lithium-sulfur (Li-S) batteries are promising candidates for next generation electrical energy storage devices due to their high specific energy. Despite intense research, there are still a number of technical challenges in developing a high performance Li-S battery. To elucidate the issues, an all solid-state Li-S battery was fabricated using Li_3PS_4 solid electrolyte. Most of the theoretical capacity of sulfur, 1600 $mAhg^{-1}$ was attained in the initial discharge-charge cycles with a high coulombic efficiency approaching 99%. To verify the benefit of the solid state electrolyte, galvanostatic stripping-deposition tests were also carried out on a symmetrical Li/Li cell and compared with those of a liquid electrolyte (1 M- lithium bis(trifluoromethane sulfonyl) imide (LiTFSI) in a mixture of 1,3-dioxolane (DOL)-diethoxyethane (DEE)). The kinetics and thermodynamics of the solid-state cell are discussed from the viewpoint of the charge transfer processes. This study demonstrates both the merits and drawbacks of using the solid sulfide electrolyte in a Li-S battery and facilitates the further improvement of this important high energy storage device.
 [DOI: 10.1149/2.0441504jes]

Manuscript submitted November 18, 2014; revised manuscript received December 24, 2014. Published January 24, 2015. This was Paper 502 presented at the Como, Italy, Meeting of the IMLB, June 10–14, 2014.

Lithium-sulfur (Li-S) batteries are attracting growing interest owing to their high specific energy above 3000 $Whkg^{-1}$ (active material). However, before this technology can be used in practice, there are some significant challenges to overcome, including red-ox shuttle of polysulfides as well as poor lithium cycle performance.

The polysulfide redox shuttle originates from the dissolution of the cathode material into the organic electrolyte. So far, various approaches have been suggested to solve the red-ox shuttle issue. $LiNO_3$ is a well-known additive for optimizing the solid electrolyte interphase (SEI) on lithium metal electrode, such as to block the deposition of polysulfides.[1,2] An ionommer (e.g., Nafion) has also been proposed for preventing the polysulfide migration[3] and a buffer solution containing polysulfides can facilitate a good cycle ability as well.[4]

The poor lithium cycle performance is due to the consumption of lithium metal during the charge-discharge process. It is well known that the lithium cycling response is primarily determined by the type of electrolyte to which it is in contact.[5,6] In the development of lithium-metal secondary batteries the *Figure of Merit* (FOM) is the parameter used to evaluate the lithium cycling ability.[5,6] Although lithium metal has a high specific capacity of 3862 $mAhg^{-1}$, its effective degree of utilization (i.e., the lithium loss relative to the amount of total input lithium metal) has to be taken into account. Generally, a valid parameter to determine the cycle ability of the lithium anode is the efficiency. For instance, it is difficult to achieve an efficiency higher than 99% for lithium cycling in a typical liquid electrolyte cell due to losses during its dissolution-deposition reaction. Therefore, the improvement of the FOM of a liquid electrolyte Li-S battery has been a major challenge to enhance the charge-discharge cycle performance and energy density of Li-S batteries.

Solid-state electrolytes, based on both inorganic and organic compounds, are valid alternatives to develop lithium batteries with high safety and long cycle life, as in fact practically demonstrated. A good example is the thin film solid-state battery adopting LIPONB (Boron doped lithium phosphorous oxynitride) which has shown a long cycle life.[7] Solid polymer batteries, having good stability and cycle performance, have also been proposed.[8] It is important to point out that these "solid-state batteries" have the favorable characteristic of avoiding lithium dendrite deposition and hence, of preventing short circuits, in cells using lithium metal as the anode active material. In addition, solid electrolytes are expected to be safer than common non-aqueous electrolyte media, because of their low or negligible vapor pressure. Recently, a class of sulfide solid electrolytes, as for instance $0.5Li_2S$-$0.5SiS_2$;[9] $0.7Li_2S$-$0.3P_2S_5$[10] and $Li_{10}GeP_2S_{12}$,[11] have attracted considerable practical interest due to their high ionic conductivity and easy mechanical processing and their use in solid lithium batteries has in fact been demonstrated.[12–16] In particular, solid-state Li-S batteries using sulfide-based solid electrolytes and Li-In or $Li_{4.4}Ge$ alloy as anode have been reported.[17–21] However, due to its high cost and high electrochemical potential (+0.62 V versus Li/Li^+) indium is not a suitable alloy electrode material since its use ultimately depresses the energy density of the battery. Considering that lithium dendrites may grow upon cycling through the cracks in the solid electrolyte, then inducing electrical short circuits, it is difficult to use lithium metal anode in contact in a pelletized electrolyte cell.[22] Therefore, avoiding dendrite formation in this type of cell is an important challenge. Spatial gaps may in fact exist in between the primary and secondary particles, and they may facilitate the dendrite growth. In a previous work, we have demonstrated a solid-state Li-S battery based on $0.8Li_2S$-$0.2P_2S_5$ electrolyte.[23] However, even cycling under shallow depth of discharge (DOD), dendrite short circuits were indeed observed.

In this work we have extended the investigation, by developing and testing a solid-state Li-S battery using a stoichiometric composition of $0.75Li_2S$-$0.25P_2S_5$, Li_3PS_4 as the electrolyte. We here demonstrate that the battery delivers a capacity of 1600 $mAhg^{-1}$ (with respect to sulfur) with a good cycling retention. We believe that this result will significantly contribute the progress of the Li-S battery technology.

Experimental

Synthesis of Li_3PS_4 and the pellet fabrication.— The sulfide solid electrolyte, $0.75Li_2S$-$0.25P_2S_5$ (stoichiometric Li_3PS_4), was prepared by using the high energy ball milling method. Li_2S (Alfa, purity 99.9%) and P_2S_5 (Aldrich, purity 99.9%) (in a molar ratio of 75:25) were placed into an argon gas filled zirconium pot with 10 and 3 mm ZrO_2 balls (7 and 10 balls, respectively) and a grinding bowl fastener

*Electrochemical Society Active Member.
**Electrochemical Society Fellow.
[d]Present address: Tokyo University of Agriculture & Technology 2-24-16 Nakacho, Koganei, Tokyo 184-8588, Japan.
[z]E-mail: yuichi.aihara@samsung.com

P-7 (Fritsch, Germany) were used. The Li_3PS_4 powder was milled at 380 rpm for 35 h. The crystal structure of the product was verified using X-ray diffraction (XRD) and Raman spectroscopy.

The solid electrolyte powder (300 mg) was put into a ϕ13 mm die, and pressure of 4 tons was applied at 25°C for 30 s using a hydraulic press. The density of the solid electrolyte pellet was 1.64 $g \cdot cm^{-3}$ at room temperature (24°C). The pellet was used for determining the ionic conductivity and charge transfer resistance of the electrolyte layer.

Fabrication of the electrochemical cells.— Preparation of the electrode materials.—The cathode composite was made from mixing sulfur powder (purity 99.5%, Sulfax PS, Tsurumi Chemical, Ibaraki) and carbon nano fibers (CNF, diameter 200 – 300 nm with an aspect ratio of 50∼100) in the ratio of 3:1 (w/w) using a mortar. Prior to the mixing, the sulfur powder and CNF were dried at room temperature and 60°C under vacuum, respectively, to remove any possible moisture or contaminant. Then Li_3PS_4 powder (60 wt%) and the sulfur/carbon fiber mixture (40 wt%) were mixed using a mortar (hence the net sulfur content in the composite is 30.0 wt%) for preparing the cathode-Li_3PS_4 composite.

A lithium foil (purity 99.8%, thickness 100 μm, Honjo metal, Osaka) was cut into disks (11 mm diameter) and used in both the Li/Li_3PS_4/S full and the Li/Li_3PS_4/Li symmetrical cells. An indium foil (4N, thickness 50 μm, Nilaco, Tokyo) was similarly cut into disks (13 mm diameter) and used for the current collectors of the In/Li_3PS_4/In blocking symmetrical cells to determine the temperature dependence of the ionic conductivity.

All the above procedures were performed in an argon filled glove box (MBRAUN Lab master, H_2O, $O_2 < 0.1$ ppm) to avoid exposure to air to prevent possible degradation of the material.

Fabrication of the cells for galvanostatic measurements and cyclic voltammetry.—A Li/Li_3PS_4/S cell was fabricated using the metal housing test cell for galvanostatic measurements. The construction of the test cell is given in the literature.[17] Li_3PS_4 (100 mg) was spread onto a stainless steel (SUS316, hereinafter SUS) cylinder surrounded by an outer insulator tube (polyoxymethylene, POM) and was pressed by hand. This procedure forms a Li_3PS_4 layer, which separates the cathode and the anode. Then 3.3 mg of the cathode powder composite (described in preparation of the electrode materials section) was uniformly spread on the solid electrolyte layer. Therefore, the active area of the cathode was around 1.33 cm^2 (same as the inner diameter of the insulator tube). After the cathode current collector (SUS cylinder) was placed onto the cathode, the lithium foil for the anode was put onto the opposite side of the pellet, and sandwiched by the two stainless steel cylinders, which work as current collectors. All the cell components were compressed together and completely pelletized by using a hydraulic press under the same conditions as for the pelletizing procedure of the solid electrolytes. After closing the metal housing cell, a screw was fastened at 3.0 Nm using a preset torque wrench to maintain the electrochemical contact in the cell. The top current collector served as the negative electrode. The upper and lower halves of the cells were electrically isolated by an O-ring.

For cyclic voltammetry (CV) measurements, an asymmetrical cell of Li/Li_3PS_4/SUS was prepared. The SUS current collector was directly attached as the working electrode. The preparation process was the same as above, except for the lack of the sulfur cathode.

In the end, each cell was bagged in an aluminum laminate and vacuum sealed to avoid exposure to air.

Fabrication of a symmetrical lithium non-blocking and an indium blocking electrodes.—Apart from the full cell preparation, two additional electrolyte pellets were made (see Synthesis of Li_3PS_4 and the pellet fabrication Section) for the fabrication of symmetrical cells. The same die as the full cell was used and carefully prepared to ensure that it has a flat contact surface by using a die. The thickness of each electrolyte pellet was designed to be thicker than that of the full cell to maintain the disk like shape. One of the electrolyte pellets was sandwiched by lithium foil electrodes (11 mm diameter and area of 0.95 cm^2) for a symmetric non-blocking cell. Another cell was prepared using an indium electrode of the same dimension for a blocking cell. The above electrode/electrolyte assemblies were placed in metal housing test cells. Similar to the full cell, the screw was fastened at 3.0 Nm to maintain the electrochemical contact in the cell after closing the metal housing. These symmetric cells were used for determining the temperature dependence of the ionic conductivity (indium blocking) and for evaluating the galvanostatic cycle (lithium non-blocking).

As before, both kinds of cells were placed in aluminum laminated bags and vacuum sealed.

Preparation of a reference liquid electrolyte Li/Li symmetrical cell.—To compare the exchange current densities of Li^0/Li^+ in the solid electrolyte and the liquid electrolyte, a 2032 coin cell was prepared and the temperature dependence of the charge transfer resistance was measured. As a liquid electrolyte, 1 M LiTFSI was dissolved in 1:1 (v/v) mixture of DOL-DEE. All the chemicals were of lithium battery grade and were purchased from Tomiyama Pure Chemical Industries (Tokyo). A glass filter (Whatman, GF/A, 0.29 mm thickness) was used as a separator. The entire procedure was performed in an argon filled glove box (MBRAUN Lab master, H_2O, $O_2 < 0.1$ ppm).

Electrochemical measurements.— Electrochemical impedance spectroscopy (EIS) was performed on the In/Li_3PS_4/In blocking, and Li/Li_3PS_4 (or 1 M-LiTFSI DOL/DEE)/Li non-blocking cell to determine the temperature dependence of both the ionic conductivity and the exchange current density using an AUTOLAB PGSTATM101 (Metrohm Autolab B.V., Utrecht) controlled by a personal computer. A temperature chamber SU-241 (ESPEC, Osaka) was also controlled by the personal computer, and was synchronized with the EIS measurement through an RS-232C under the NOVA software suite (Metrohm Autolab B.V.). After the cells were set in the temperature chamber and connected to the measurement cables, the temperature was once increased to 40°C (for Li/Li) and 80°C (for In/In), and kept for one hour. Then the EIS was performed in the frequency range 1 MHz – 0.01 Hz with ±10 mV perturbation versus open-circuit potential at 5°C increments down till −20°C. At each temperature, a rest time was set for one hour to reach equilibrium before the measurements. The impedance spectra were analyzed using ZSimpWin ver.3.21 software (EChem Software, Michigan).

Galvanostatic deposition/stripping cycle (Galvanostatic square wave) was performed on a Li/Li_3PS_4(or 1 M-LiTFSI DOL/DEE)/Li cell using a Solartron SI 1260 impedance analyzer equipped with a Solartron 1470E cell test system (Solartron analytical, UK). Cyclic voltammetry was performed on a Li/Li_3PS_4/SUS cell using an AUTOLAB PGSTATM101 controlled by a personal computer. The cells were contained in a temperature chamber (SU-241, Espec, Osaka), and the measurements were carried out with a potential sweep from −0.5 to 1.0 V with a scanning rate of 10 mVs^{-1} at 25°C.

The Galvanostatic discharge-charge cycle was performed for the full cell using a battery tester, TOSCAT-3000 (Toyo system, Fukushima) at 1/50C (0.025 $mAcm^{-2}$) rate. The cut off voltages for the cycle test were set at 2.6 and 1.3 V for charge and discharge, respectively.

Analytical methods.— The powder X-ray diffraction (XRD, CuKα, 45 kV, 40 mA) pattern was measured using an Empyrean XRD system (PANalytical, Almelo) for verifying the amorphous structure of Li_3PS_4 at room temperature. An Ar-gas-filled sample holder was used to prevent degradation due to moisture.

Raman spectra of the Li_3PS_4 powders were observed by using a near-infrared FT-Raman spectrometer (JASCO, NRS-3100, Tokyo). A green laser of 532 nm wavelength was used.

Results and Discussion

Characterization of the Li_3PS_4 solid electrolyte.— The structure analysis of the electrolyte sample was performed using XRD and Raman spectroscopy. The XRD pattern of the synthesized Li_3PS_4 powder

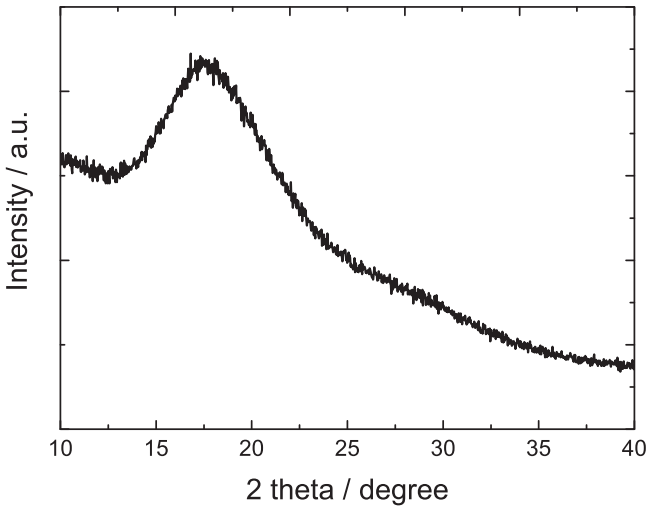

Figure 1. XRD diffraction pattern of the Li_3PS_4 (CuKα, 45 kV, 40 mA).

is amorphous (see Figure 1), as expected since the sample was not annealed. Considering that no peaks matching the starting material, Li_2S and P_2S_5, were observed, we conclude that a stoichiometric reaction did indeed take place to form the Li_3PS_4 electrolyte. The Raman spectroscopy spectrum of Li_3PS_4 showed a sharp peak around 421 cm^{-1} (see Figure 2) which was ascribed to the stretching of PS_4^{3-}.[10] Since this anion is the predominant species observed in the Raman spectrum, we may confirm that the stoichiometric composition of the synthesized powder, $0.75Li_2S0.25P_2S_5$ (molar ratio) is that of amorphous Li_3PS_4. However, a small shoulder peak was observed around 387 cm^{-1} indicating that a dimer, $P_2S_6^{4-}$ anion might also exist as a minor component in the solid electrolyte resulting from its inhomogeneous (in terms of primary and secondary particle sizes) high energy ball milling preparation. Unfortunately, the presence of impurities makes it difficult to obtain reproducible ionic conductivity data, especially for measurement of a pelletized disk, due to the fact that they strongly depends on the density of the tested material.[23] In fact, different activation energy values have been reported for this type of electrolyte materials.[24,25]

Lithium ion conductivity.— Li_3PS_4 is a single ion solid conductor and, as such, its mechanism of ionic transport is quite different from that occurring in liquid electrolytes. The temperature dependence of

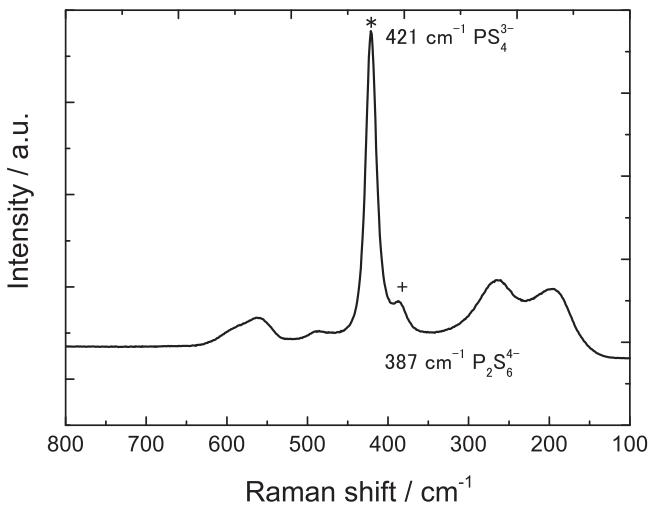

Figure 2. Raman spectrum of the Li_3PS_4 powder sample. The 532 nm green laser was used for the excitation.

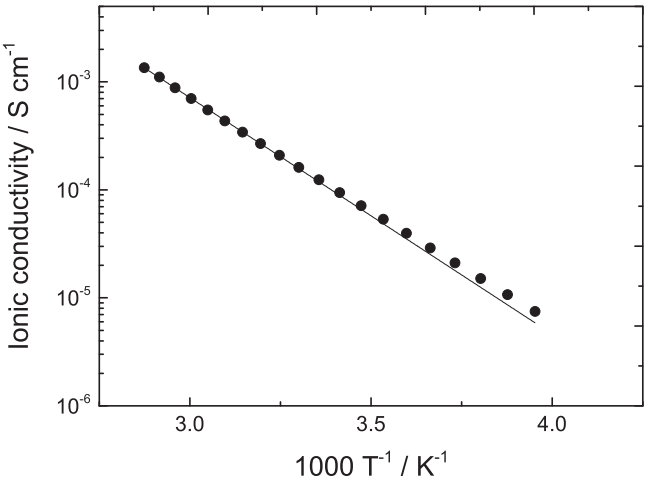

Figure 3. Temperature dependence of the lithium ion conductivity of the Li_3PS_4 solid electrolyte. The solid line is the linear regression to the Arrhenius plot.

the lithium ion conductivity of Li_3PS_4 evolved with typical Arrhenius trend extending from −20 to 80°C, with an apparent activation energy of 41.9 $kJmol^{-1}$. (See Figure 3.) This activation energy value, although higher than that reported in a crystalline phase of sulfide solid electrolytes,[24] is still reasonable if compared with values obtained for other amorphous phases.[26] The lithium ion conductivity of our Li_3PS_4 sample was found to be on the order of 10^{-4} Scm^{-1}. This is approximately two orders of magnitude lower than that of a typical liquid electrolyte.[29] Although the ionic conductivity of the amorphous Li_3PS_4 is lower than typical liquid electrolytes, the value is reasonably high among the existing solid electrolytes.[11,30] Furthermore, the gap between solid and liquid electrolytes is now becoming smaller due to the recent development of the solid ion conductors. For instance, 12 $mScm^{-1}$ of the lithium ion conductivity has been obtained in sulfide base electrolyte, $Li_{10}GeP_2S_{12}$, at room temperature.[11] Moreover, there is an advantage of the high transport number of the inorganic solid electrolyte over the liquid. The net lithium ion transport numbers of typical liquid electrolytes are less than half of that of the solid Li_3PS_4.[27,28] These considerations imply that there is a good chance that the solid electrolyte will show good performance with unique advantages over the liquid electrolyte batteries.

We should note that a significant challenge for the solid electrolyte materials is the high activation energies of the ionic conductivities. However, we believe that these high activation barriers cannot be typical of the bulk of the material, but rather associated to grain boundaries and inhomogeneous composition of the compressed powder sample.

Lithium stripping-deposition studies.— To investigate the deposition-stripping phenomena of the lithium metal electrode, cyclic voltammetry was performed on a Li/Li_3PS_4/SUS asymmetrical cell. Figure 4 shows the result of this test. The smooth lithium deposition-stripping behavior onto the SUS working electrode was confirmed by the trend of the voltammogram. At the first cycle, overpotential for the lithium deposition was slightly larger than at later cycles, due to the existence of the SEI film, consisting of lithium inorganic compounds on the lithium surface (hereinafter, native SEI). After three cycles, the lithium deposition process in the cathodic scan was matched with the stripping process in the reverse anodic scans with a very good reversibility

(Above mentioned passivation film is generally called the solid electrolyte interphase (SEI) in a liquid electrolyte system. However, recently the use of the same terminology is extended to the solid electrolyte systems, in particular for the systems with Li metal electrode.[31–33] We follow this convention in the field and adopt in this paper.)

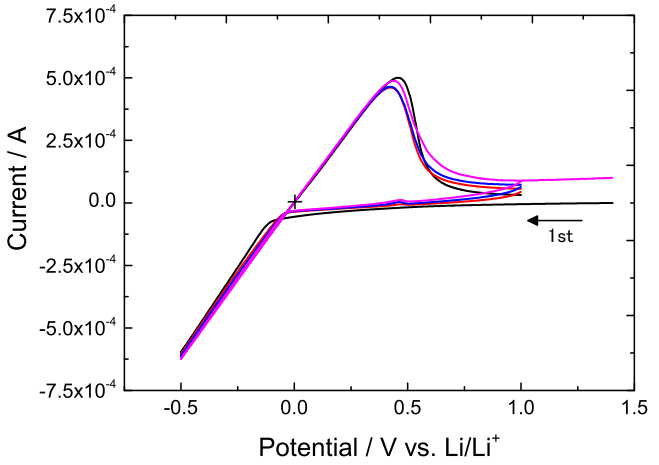

Figure 4. Cyclic voltammetry of the Li_3PS_4 solid electrolyte at 25°C. The black, red, blue, and pink curves refer to the 1st, 3rd, 5th, and 10th cycle, respectively. Potential range: 0.5 −1.0 V. Scanning rate: 10 mVs^{-1}. Working electrode: SUS316, Counter and reference electrode: lithium.

The lithium red-ox process was further investigated by galvanostatic deposition-stripping cycles using the symmetric lithium electrode cells. The results for the solid and liquid electrolytes are shown together for comparison in Figure 5. The two voltage profiles match very well qualitatively, with no sign of polarization observed during the test, although the overpotential of the solid electrolyte cell is larger since in this case the process is mostly governed by iR drop and the resistance R of the solid is higher than that of the liquid.

EIS was performed on the same symmetric lithium electrode cells before and after the galvanostatic deposition-stripping test with the aim of determining the related charge transfer resistance. Nyquist plots of the solid and liquid electrolyte cells at −20°C are shown in Figures 6a. For the liquid electrolyte cell, the expected typical impedance spectrum involving a solution (or bulk) resistance (R_b), an interfacial resistance corresponding to the charge transfer resistance (R_{CT}), and a diffusion resistance (R_W) is observed. In contrast, the solid electrolyte cell (blue squares) shows a different frequency response where the resistance is composed of R_b (with an associated capacitance C), R_{CT} and R_W. For their comparison, the impedance responses of the liquid and solid electrolyte cells were analyzed using the following equivalent circuits: $R_b(R_{CT}Q_{CT})Q_D$ and (R_bQ_b) $(R_{CT}Q_{CT})Q_D$, respectively. A constant phase element (Q) was adopted to fit the data. At −20°C, the R_{CT} of the liquid electrolyte cell is much larger than

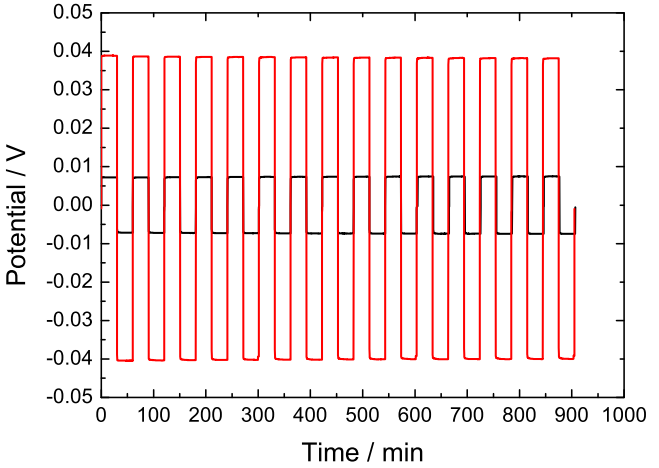

Figure 5. Galvanostatic lithium deposition-stripping square wave sequence for a solid electrolyte (red) and a liquid electrolyte (black) symmetrical Li/Li cell. Current pulse: +/− 0.2 $mAcm^{-2}$.

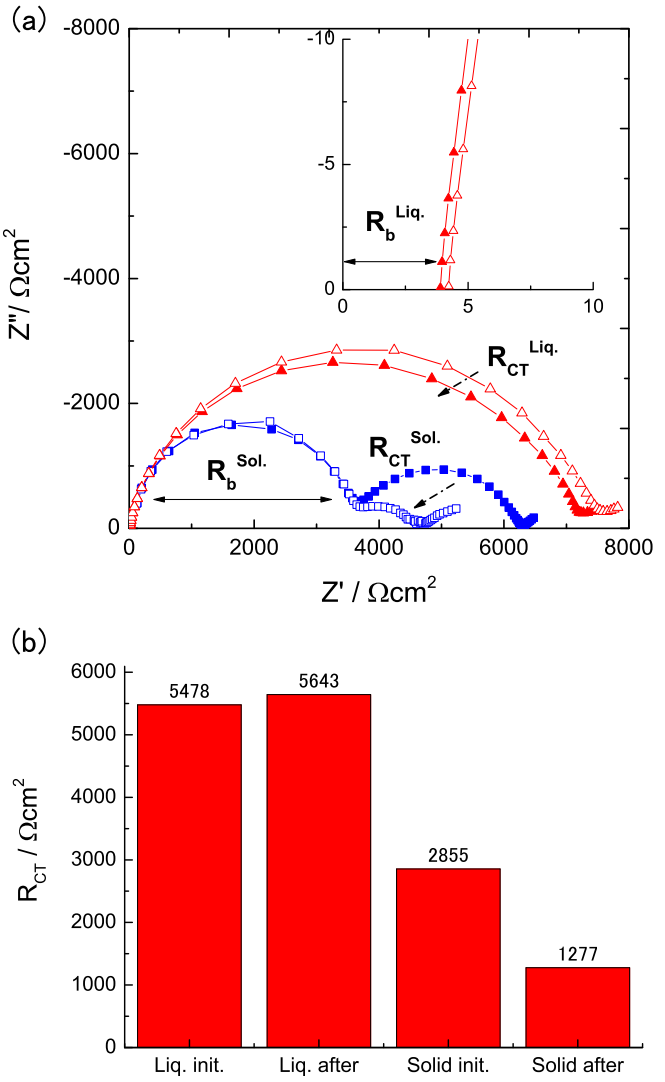

Figure 6. (a) Nyquist plots of solid (blue) and liquid (red) electrolyte symmetrical Li/Li cells at −20°C. The solid and open symbols correspond to the data before and after stripping-deposition, respectively. (b) R_{CT} for both liquid and solid electrolyte cells before and after the stripping-deposition cycles.

that of the solid electrolyte cell. The estimated R_{CT} for both liquid and solid electrolyte cells are shown in the Figure 6b. It is clear from the figure that impact of the stripping was negligible for the liquid electrolyte, but the clear difference was observed for the solid electrolyte sample. It should be noted that the frequency response of the latter exhibited little temperature sensitivity and that the response during the charge transfer process of the former became slower at the lower temperature. This is probably because, due to the nature of the liquid electrolyte, its carrier number and reorientation energy are governed by the thermodynamics of the liquid solution. This effect was clearer on the impedance plot at the lower temperature although similar trend was also seen at 25°C.

The temperature dependence of the exchange current density (i_0) was estimated before and after the SEI stripping process at each temperature T according to the equation:

$$i_0 = \frac{RT}{R_{CT}nF}, \qquad [1]$$

where the R and F are the Gas and Faraday constants, respectively, and n is the valence of the charge carrier, in this case, +1 for Li^+, obtaining the Arrhenius trend reported in Figure 7. From this plot, the activation energy of i_0 was determined to be in the 68.4 to

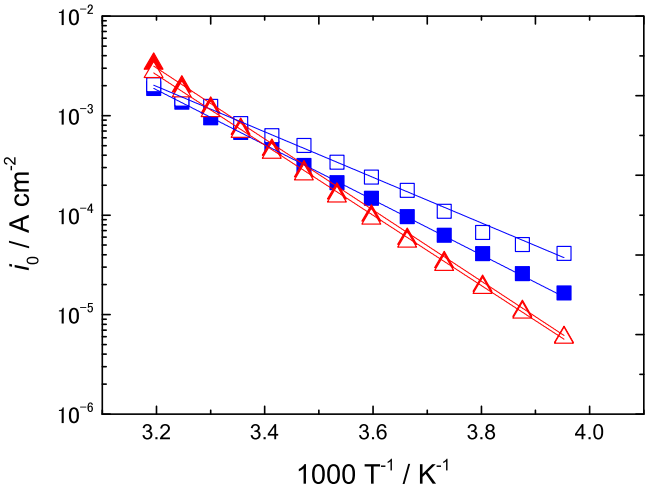

Figure 7. Temperature dependence of the exchange current density i_0 for a Li/Li$^+$ redox couple in the Li_3PS_4 solid (blue squares) and the liquid (red triangles) electrolytes. The solid and open symbols refer to i_0 before and after after a Galvanostatic stripping-deposition cycle, respectively.

67.6 kJmol^{-1} range for the liquid cell and in the 52.1 to 44.5 kJmol^{-1} range for the solid cell.

The values of i_0 increased at each temperature for both liquid and solid electrolyte cells after the SEI stripping, possibly as a consequence of the increase of the active lithium electrode surface area resulting from the newly deposited lithium. This native SEI is generally recognized as a primary SEI formed by inorganic gases during preparation and storage process of lithium foil. Generally, in a liquid electrolyte, it is well known that the secondary SEI based on the decomposition components of an organic electrolyte, is formed on the inorganic primary SEI.[31–33] The value of the activation energy did not appreciably change in the liquid cell where only a small reduction from 68.4 to 67.6 kJmol^{-1} (1.6%) was observed. On the contrary, in the solid cell the activation energy decreased from 52.1 to 44.5 kJmol^{-1}, i.e., nearly 14.6% after the deposition-stripping cycle. This may be due to the fact that the native SEI stripping may have altered the charge transfer process, i.e., passing from Li_3PS_4 ↔ SEI ↔ Li/Li$^+$ to Li_3PS_4 ↔ Li/Li$^+$.

The number of the charge carriers in the electrolytes also have an influence on the i_0 at each temperature. At 25°C, this number should be 6.0 × 10^{20} for the liquid electrolyte and 5.6×10^{21} for the solid Li_3PS_4 electrolyte. It is assumed that all Li-ions contribute to the conduction for the solid electrolyte, but it is not the case for the liquid electrolyte due to the occurrence of strong ion association, especially at low temperatures. The combination of activity coefficient (solution side), SEI (surface) and solvation-desolvation process (interface) is thought to be responsible for the higher E_a value observed in the liquid electrolyte in comparison with that in the solid.

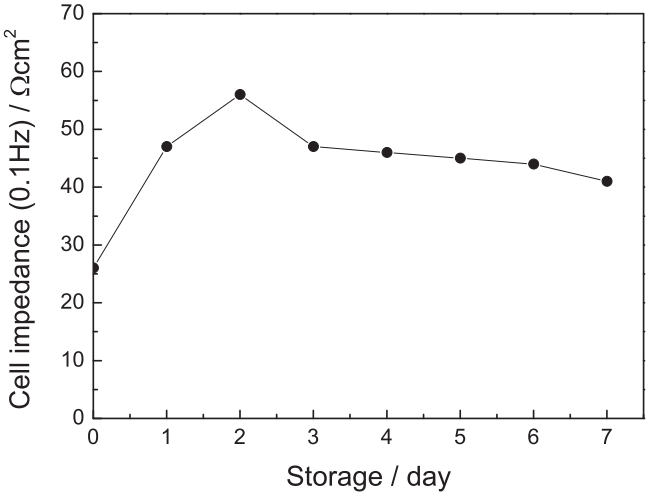

Figure 8. Cell impedance evolution of the Li/Li_3PS_4/Li symmetrical cell at 80°C for seven days. The impedance was taken at 0.1 Hz.

Table I. Specification of the Li-S test cell.

Cell specification	
Cathode sulfur weight fraction	30 wt%
Cathode composite loading	2.5 mgcm^{-2}
S/C (w/w)	3
Net sulfur loading	0.75 mgcm^{-2}
Cell capacity	1.2 mAh
Cathode specific capacity (active area: 13 mmΦ)	0.82 mAhcm^{-2}
Anode specific capacity (active area: 11 mmΦ)	17.3 mAhcm^{-2}
Utilization of anode for 100% DOD (1600 mAhg^{-1})	∼5%

Stability of Li_3PS_4 with the lithium metal on storage.— To verify the chemical stability of the solid electrolyte against lithium metal, EIS was performed on a Li/Li_3PS_4 /Li symmetrical cell kept at 80°C for a week. Prior to the EIS storage test, a galvanostatic stripping-deposition cycle was done on the cell to obtain a clean lithium surface. The time evolution of the cell resistance at 0.1 Hz is given in Figure 8. The cell impedance once increased within the first 24 hours, and became almost constant after 2 days. Since it was difficult to analyze the impedance spectra at 80°C due to the distorted shape, the formation of a passivation film could not be clearly identified. However, a passivation reaction must have occurred at the initial stage, and increased the cell impedance. This indicate that the chemical stability of the synthesized Li_3PS_4 electrolyte was not sufficient to apply to the lithium metal electrode.

Li/Li_3PS_4/S full cell.— A Li/Li_3PS_4/S solid-state cell was assembled and tested. Its details are given in Table I. The voltage profiles of the charge-discharge curves at 25°C and 80°C are shown in Figure 9. The result clearly showed that full specific capacity of sulfur ∼ 1600 mAhg^{-1} (0.05 C, 0.025 mAcm^{-2}) was achieved at both temperatures. Importantly, the initial coulombic efficiency approached 99%, confirming the benefit in using lithium metal as anode. We also conclude that the high value of the coulombic efficiency is a clear evidence that polysulfide shuttle was prevented by the solid electrolyte layer. This is clearly an advantage of using a solid electrolyte since

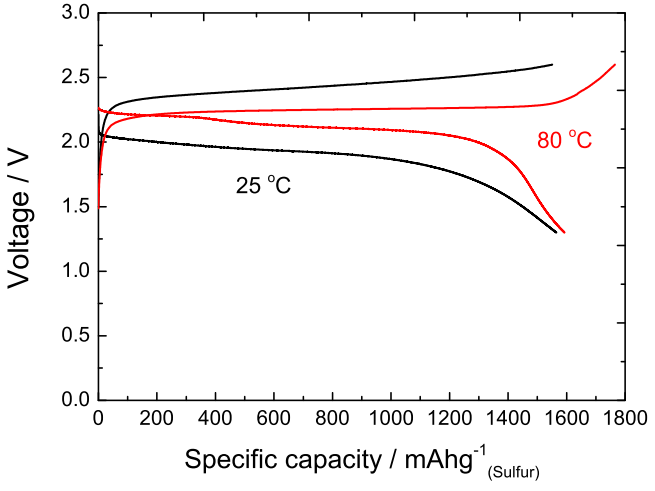

Figure 9. Voltage profiles of charge-discharge cycles of the Li/Li_3PS_4/S battery. Current density j = 0.025 mAhcm^{-2} (= 0.05 C); temperature: 25 °C (black lines) and 80 °C (red lines). The specific capacity is given per g of sulfur.

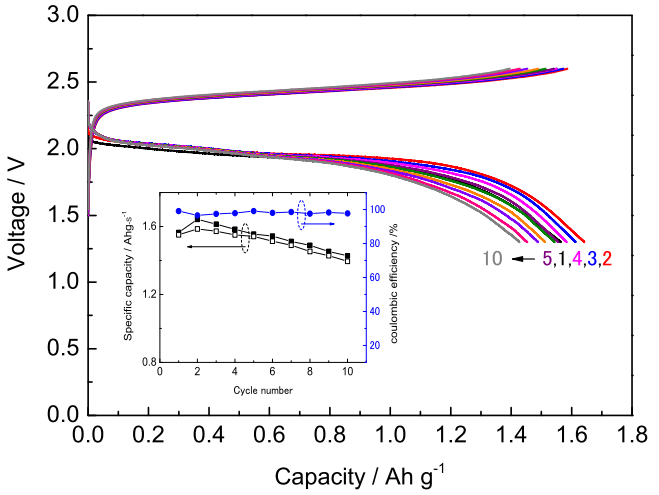

Figure 10. Voltage profiles of the charge-discharge cycles of the Li/Li_3PS_4/S cell at 25°C. Current density $j = 0.025$ mAhcm^{-2} (= 0.05C). The colored numbers (1,2,3,4,5 and 10) indicate the corresponding charge discharge cycle. The inset figure shows the cell discharge (solid square) /charge capacity (open square) and coulombic efficiency (solid circle) at each cycle.

it can physically block the migration of the polysulfide shuttle from the electrode. In general, consumption of the lithium occurrs in the Li-S batteries due to the polysulfide shuttle red-ox reaction. Therefore the coulombic efficiency is usually quite poor. The reaction mechanism in a conventional LIB is completely different (i.e. intercalation-de-intercalation reaction) and the efficiency never reaches 98–99% without additives.[34–36]

Another important remark is that the discharge plateau typically reported for Li-S batteries was not seen at 25°C where a large discharge-charge polarization was also observed. The electrochemical reaction was significantly accelerated at 80°C, where the cycling nearly evolved along the expected plateau. Although the reaction in the solid electrolyte Li-S cell is still unclear, its kinetics are expected to be much slower in the liquid electrolyte cell.

A cycle test was performed on the Li/Li_3PS_4/S cell at 25°C and 0.025 mAhcm^{-2}. The results are shown in Figure 10. The number of cycles performed in this study is too short to accurately compute the FOM. However, the cycle life of the all solid-state Li-S battery can still be estimated from the lithium consumption. Using the coulombic efficiency (E_{cf}) of 98.0%, the FOM can be roughly estimated by the equation:

$$\text{FOM} = 1/\left(1 - \frac{E_{cf}}{100}\right). \quad [2]$$

This gives the FOM to be 50 and, considering that the anode utilization is approximately 5%. (See Table I) From this one can assume the life of our Li/Li_3PS_4/S solid-state cell should be approximately 1000 cycles (DOD100%). Realistically, the risk of dendrite formation and of cathode and electrolyte degradation cannot be excluded and they might shorten the cycle life of the battery. Long cycle life and high coulombic efficiency have been reported for thin film lithium batteries where the electrolyte layers are generally prepared by a vapor deposition process and are quite dense.[7] This suggests that a dense solid electrolyte is a key for making a high performance solid state battery.

Conclusions

A novel all solid-state Li-S battery was fabricated and evaluated by a number of tests. We showed that this battery benefits by a series of favorable properties, including a smooth stripping-deposition of lithium, a capacity approaching the theoretical value and, most importantly, an initial charge-discharge coulombic efficiency approaching 99% (the average in ten cycles is 98%). In addition, the activation energy of the charge transfer process was 44.5 kJmol^{-1} which was much smaller than that of a corresponding liquid electrolyte Li-S cell.

These results are convincing in demonstrating that the solid electrolyte is very effective in physically preventing polysulfide migration. Overcoming the polysulfide shuttle is a significant advantage since it is a major drawback for a typical liquid electrolyte based Li-S battery. Further work is in progress in our laboratories to elucidate the behavior of our battery, and also to improve its construction. Nevertheless, we believe that the data here reported, even if still at a preliminary stage, are of importance for the progress of the lithium-sulfur battery technology.

Acknowledgment

The authors acknowledge the Samsung Advanced Institute of Technology for funding this research. The authors greatly appreciate the help from Prof. William S. Price to improve the quality of the manuscript.

References

1. D. Aurbach, E. Pollak, R. Elazari, G. Salitra, C. S. Kelley, and J. Affinito, *J. Electrochem. Soc.*, **156**, A694 (2009).
2. R. Elazari, G. Salitra, Y. Talyosef, J. Grinblat, C. Scordilis-Kelley, A. Xiao, J. Affinito, and D. Aurbach, *J. Electrochem. Soc.*, **157**, A1131 (2010).
3. I. Bauer, S. Thieme, J. Brückner, H. Althues, and S. Kaskel, *J. Power Sources*, **251**, 417 (2014).
4. D.-J. Lee, M. Agostini, J.-W. Park, Y.-K. Sun, J. Hassoun, and B. Scrosati, *ChemSusChem*, **6**, 2245 (2013).
5. K. M. Abraham, J. S. Foos, and J. L. Goldman, *J. Electrochem. Soc.*, **131**, 2197 (1984).
6. S. Tobishima, M. Arakawa, T. Hirai, and J. Yamaki, *J. Power Sources*, **20**, 293 (1987).
7. B. Fleutot, B. Pecquenard, F. Le Cras, B. Delis, H. Martinez, L. Dupont, and D. Guy-Bouyssou, *J. Power Sources*, **196**, 10289 (2011).
8. Y. Aihara, J. Kuratomi, T. Bando, T. Iguchi, H. Yoshida, T. Ono, and K. Kuwana, *J. Power Sources*, **114**, 96 (2003).
9. J. H. Kennedy, S. Sahami, S. W. Shea, and Z. Zhang, *Solid State Ionics*, **18–19**(Part 1), 368 (1986).
10. F. Mizuno, A. Hayashi, K. Tadanaga, and M. Tatsumisago, *Adv. Mater.*, **17**, 918 (2005).
11. N. Kamaya, K. Homma, Y. Yamakawa, M. Hirayama, R. Kanno, M. Yonemura, T. Kamiyama, Y. Kato, S. Hama, K. Kawamoto, and A. Mitsui, *Nat. Mater.*, **10**, 682 (2011).
12. K. Takada, K. Iwamoto, and S. Kondo, *Solid State Ionics*, **117**, 273 (1999).
13. N. Ohta, K. Takada, L. Zhang, R. Ma, M. Osada, and T. Sasaki, *Adv. Mater.*, **18**, 2226 (2006).
14. A. Sakuda, A. Hayashi, and M. Tatsumisago, *J. Power Sources*, **195**, 599 (2010).
15. N. Machida, J. Kashiwagi, M. Naito, and T. Shigematsu, *Solid State Ionics*, **225**, 354 (2012).
16. A. Sakuda, A. Hayashi, and M. Tatsumisago, *Sci. Rep.*, **3**, 2261 (2013).
17. S. Ito, S. Fujiki, T. Yamada, Y. Aihara, Y. Park, T. Y. Kim, S.-W. Baek, J.-M. Lee, S. Doo, and N. Machida, *J. Power Sources*, **248**, 943 (2014).
18. M. Nagao, A. Hayashi, and M. Tatsumisago, *Electrochim. Acta*, **56**, 6055 (2011).
19. M. Nagao, A. Hayashi, and M. Tatsumisago, *J. Mater. Chem.*, **22**, 10015 (2012).
20. N. Machida, K. Kobayashi, Y. Nishikawa, and T. Shigematsu, *Solid State Ionics*, **175**, 247 (2004).
21. N. Machida, H. Yamamoto, S. Asano, and T. Shigematsu, *Solid State Ionics*, **176**, 473 (2005).
22. M. Nagao, A. Hayashi, M. Tatsumisago, T. Kanetsuku, T. Tsuda, and S. Kuwabata, *Phys. Chem. Chem. Phys.*, **15**, 18600 (2013).
23. M. Agostini, Y. Aihara, T. Yamada, B. Scrosati, and J. Hassoun, *Solid State Ionics*, **244**, 48 (2013).
24. K. Homma, M. Yonemura, T. Kobayashi, M. Nagao, M. Hirayama, and R. Kanno, *Solid State Ionics*, **182**, 53 (2011).
25. N. D. Lepley, N. A. W. Holzwarth, and Y. A. Du, *Phys. Rev. B*, **88**, 104103 (2013).
26. Y. Ooura, N. Machida, T. Uehara, S. Kinoshita, M. Naito, T. Shigematsu, and S. Kondo, *Solid State Ionics*, **262**, 733 (2014).
27. Y. Aihara, T. Bando, H. Nakagawa, H. Yoshida, K. Hayamizu, E. Akiba, and W. S. Price, *J. Electrochem. Soc.*, **151**, A119 (2004).
28. K. Hayamizu, Y. Aihara, S. Arai, and C. G. Martinez, *J. Phys. Chem. B*, **103**, 519 (1999).
29. M. S. Ding, K. Xu, S. S. Zhang, K. Amine, G. L. Henriksen, and T. R. Jow, *J. Electrochem. Soc.*, **148**, A1196 (2001).
30. K. Takada, *Acta Mater.*, **61**, 759 (2013).
31. E. Peled, D. Golodnitsky, G. Ardel, and V. Eshkenazy, *Electrochim. Acta*, **40**, 2197 (1995).
32. D. Pletcher, J. F. Rohan, and A. G. Ritchie, *Electrochim. Acta*, **39**, 1369 (1994).
33. G. Zhuang and P. N. Ross Jr, *J. Power Sources*, **89**, 143 (2000).
34. X. Liang, Z. Wen, Y. Liu, M. Wu, J. Jin, H. Zhang, and X. Wu, *J. Power Sources*, **196**, 9839 (2011).
35. S. Xiong, K. Xie, Y. Diao, and X. Hong, *Electrochim. Acta*, **83**, 78 (2012).
36. S. S. Zhang, *Electrochim. Acta*, **70**, 344 (2012).